50th AIAA Aerospace Sciences Meeting including the New Horizons Forum and Aerospace Exposition
09 - 12 January 2012, Nashville, Tennessee
AIAA 2012-1291

Fabrication, Integration, and Initial Testing of a SMART Rotor*

Jonathan Berg†, Dale Berg‡, and Jon White§
*Sandia National Laboratories**, Albuquerque, NM, 87185-1124*

Sandia National Laboratories has designed and built a full set of three 9-meter blades (based on the Sandia CX-100 blade design) equipped with active aerodynamic blade load control surfaces on the outboard trailing edges. The fabrication of the blades, modifications to allow integration of the active control modules, and test results to date are presented.

I. Introduction

REDUCING ultimate and oscillating (or fatigue) loads on the wind turbine rotor can lead to reductions in loads on other turbine components such as the drive train, gearbox, and generator. This, in turn, is expected to reduce maintenance costs and may allow a given turbine to user longer blades to capture more energy. In both cases, the ultimate impact is reduced cost of wind energy. With the ever increasing size of wind turbine blades and the corresponding increase in non-uniform loads along the span of those blades, the need for more sophisticated load control techniques has produced great interest in the use of aerodynamic control devices (with associated sensors and control systems) distributed along each blade to provide feedback load control (often referred to in popular terms as 'smart structures' or 'smart rotor control'). A recent review of concepts and feasibility and an inventory of design options for such systems have been performed by Barlas and van Kuik at Delft University of Technology (TUDelft)[1]. Active load control utilizing trailing edge flaps or deformable trailing edge geometries (referred to here as Active Aerodynamic Load Control or AALC) is receiving significant attention, because of the direct lift control capability of such devices and recent advances in smart material actuator technology. Researchers at TUDelft[2-3], Risø/Danish Technical University Laboratory for Sustainable Energy (Risø/DTU)[4-10] and Sandia National Laboratories (SNL)[11-17] have been very active in this area over the past few years.

The SNL work has focused on performing extensive simulations of AALC on several turbine configurations and has analyzed the simulation results to estimate the fatigue damage reduction on the rotor and gearbox and the cost-of-energy benefits of integrating trailing edge technology into the tip region of the turbine blades. These simulation results show the potential for significant impacts on fatigue damage and cost of energy, but experimental data is badly needed to confirm the simulation-based analyses. To the best of our knowledge, no research group has yet built and field tested a rotor with a full smart blade set.

SNL has built a set of blades for its 100 kW test turbine in order to test AALC concepts. The main thrusts of this effort are to develop and validate a highly accurate structural dynamics model of the operating rotor, to work through the implementation details involved with developing appropriate control algorithms for such a rotor, and to obtain experimental verification of simulation runs; we are not attempting to design the optimal rotor for integration of AALC control capability or to develop the optimal control strategy. The design of the blade set is covered briefly in this paper and the reader is directed to a previous AIAA paper[18] for additional information. The fabrication, integration, and test results to date for this smart blade set are the subjects of this paper.

II. Blade Design

The starting point for the SMART blade design was the CX-100 research blade[19] developed by Sandia National Laboratories through collaboration with industry partners and first built in 2004. The CX-100 is a 9-meter blade

† Member of Technical Staff, Wind Energy Technology Department, Mail Stop 1124, AIAA Member.
‡ Principal Member of Technical Staff, Wind Energy Technology Department, Mail Stop 1124, AIAA Associate Fellow.
§ Senior Member of Technical Staff, Wind Energy Technology Department, Mail Stop 1124, AIAA Member.
** Sandia is a multiprogram laboratory operated by Sandia Corporation, a Lockheed Martin Company, for the United States Department of Energy's National Nuclear Security Administration under contract DE-AC04-94AL85000.

designed for a 100 kW stall-controlled turbine. The first set of these research blades underwent extensive computer modeling, structural testing, and field testing[20-22]. White, Adams, and Rumsey[23] subsequently used the design to fabricate a blade with internally mounted sensors measuring strain, temperature, and acceleration for the purpose of operational monitoring of blade loading and deflection. These research projects provided a wealth of knowledge for the current SMART rotor effort.

A schematic of the CX-100 is shown in Figure 1. The design incorporates carbon fiber spar caps which run nearly the entire length of the blade, providing increased stiffness in a key area. A single shear web, constructed of fiber glass and balsa, bridges between the blade skins underneath the spar caps. The blade skin laminate stack consists of a gel coat at the outer surface, a fiber glass mat, then a single layer of double-bias fiber glass, a 1/4 inch thick balsa core, and a second layer of double-bias fiber glass. In the following discussion, 0m span is at the blade root and 9m span is at the blade tip.

The design of the SMART blades incorporates all of the CX-100 features and includes modifications for integrating three AALC modules. We chose conventional rigid flaps to be the AALC device for this first implementation but we intentionally made the design modular so that new modules could be swapped out in the future. The blade cutout which accepts the flap modules is illustrated in Figure 1. The cutout extends 40% of chord forward of the trailing edge at span 7.029m (the inboard end) and linearly expands to 50% of chord at 8.857m (the outboard end). This cutout does not extend to the tip of the blade – the outer 14.3cm (one tip chord length) of the trailing edge is left intact to minimize the impact of the blade tip vortex on the performance of the AALC device. With these dimensions, the cutout is large enough for the modules to house the three motors which actuate the flaps and provide room for a flap width of 20% chord.

Removing this amount of material from the original CX-100 blade would have very large impacts on the structural properties of the blade in the outboard region – the lead-lag, flap, and torsional stiffnesses would all be significantly reduced. In order to minimize or eliminate those reductions, the SMART blade design replaces the outer layer of glass double-bias laminate in both the high pressure and low pressure skins with a double layer of carbon fiber double-bias laminate. As shown on Figure 1, the carbon material starts at the trailing edge at 6m and reaches the leading edge at about 6.5m, with the transition line between glass and carbon following the bias fiber direction of 45°. The inboard edges of the two carbon layers overlap the outboard edge of the fiber glass layer in the transition region to efficiently transfer the skin loads between the two skin materials.

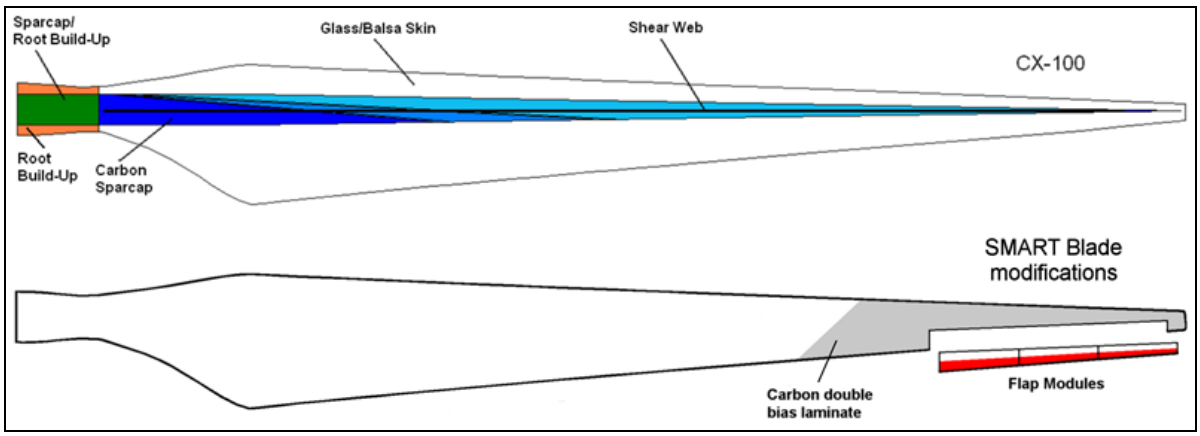

Figure 1. The SMART blade design incorporates all of the CX-100 features plus modifications for integrating three active flap modules.

The CX-100 shear web ends at approximately 8m. For the SMART design, we have added a second shear web between 7.0m and 8.8m, positioned somewhat aft of the original shear web. This aft shear web provides a mounting point for the active aero modules, facilitates the transfer of the associated loads toward the root of the blade, and helps to maintain torsional stiffness. We have also added a single rib at the inboard end of the cutout region to help transfer the loads from the aft shear web to the main shear web. The aft shear web and cutout effectively reduce the aft panel size and eliminate any concerns of buckling outboard of 7.0m, so we have removed the balsa from the skins in this area as well.

III. Flap Module Design

The aerodynamic control devices on this initial demonstration unit are 20% chord conventional flaps with +/- 20° maximum deflection. We elected the conventional flaps not because they will provide the best possible performance, but because our primary objective in this project is to build and fly a set of SMART blades. By using flaps we saved the development time and cost that would be required to miniaturize other potential control devices such as microtabs or morphing trailing edge flaps.

There are three independent control surfaces on each blade. The reasoning behind this design decision is multifaceted. First of all, space is limited at the blade tip and it is evident that the "muscle" required to drive a single flap covering 20% of blade span is more than what can be packed into any one location. In addition, independent actuation of multiple flaps is desirable, both for initial testing and for future research into distributed control. Finally, our chosen manufacturing method naturally resulted in modules of a certain size. Given the complex geometry and our need to have the ability to quickly make design iterations, rapid prototyping technology was the clear choice for fabrication. Our in-house capability is limited to parts with the largest dimension being about one foot; each flap module consists of two of these 1-foot pieces joined together. This necessitated having three modules per blade to obtain the desired length of flap.

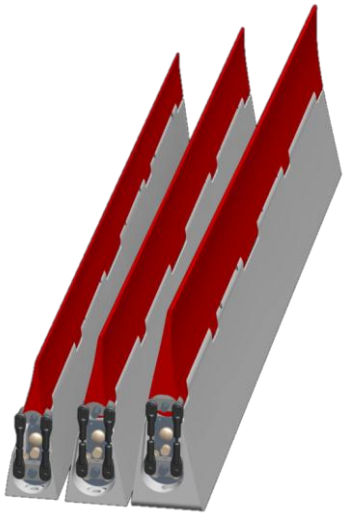

Figure 2. Each blade has a set of three flap modules.

The design of each flap module consists of two main pieces: (1) a base piece that houses the motor and mounts to the blade and (2) the flap itself that is attached to the base by a hinge as illustrated in Figure 2. The center module of the three modules on each blade also includes channels running to surface pressure taps and a mounting space for two accelerometers. To reduce weight and minimize the impact of the modules on the structural dynamic response of the blade, the base and flap were hollowed out as much as possible without sacrificing structural integrity (the skin thickness of the flap is approximately 0.06" and the wall thickness of the base is approximately 0.20"). In addition, the flap center of gravity was moved as close to the hinge as possible without adding mass, in order to minimize the possibility of inertial-driven flap flutter.

Motion of the motor shaft is transferred to the flap through a dual push/pull rod mechanism as shown in Figure 3. A rectangular control horn installed on each shaft creates the torque arms and the dual rods, which are installed with a small amount of pre-load tension, tie together the ends of the torque arms to create a parallelogram four-bar linkage.

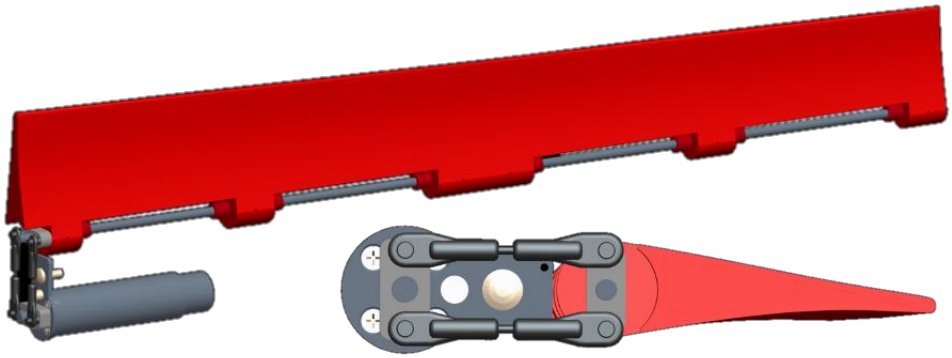

Figure 3. Detailed view of dual push/pull rod mechanism and motor (base piece is hidden).

IV. Fabrication & Integration

A. Blade Fabrication

The SMART blades skins were fabricated by TPI at their Rhode Island plant in June 2010, using their original CX-100 molds and their standard vacuum infusion process utilizing epoxy resin. In early October 2010, SNL staff traveled to the TPI plant to install an extensive instrumentation package in each blade. The performance of the SMART rotor's instrumentation array will be critical to the capabilities and performance of the active load control system. Each blade was instrumented with an internally-mounted array of accelerometer, fiber-optic strain, metal

foil strain and fiber-optic temperature sensors, as well as pressure taps and Pitot tubes. The number and locations of the accelerometers were driven by sensor optimization strategies that account for expected rotor loads, deflections, modal contributions, mass and stiffness distributions, and co-locations with other measurements for multi-physics observers.

Applying these optimizations resulted in single triaxial and uniaxial accelerometers placed at the 2m and 8m locations in each blade to permit estimation of all linear deflections and span-wise rotations. The strain sensors were located at the root, 25%, 50%, and 75% of blade spanwise distance to enable accurate capture of the curvature along the blade for the application of shape reconstruction force and deflection estimators. The measurements at these locations will also be used to train a modal filter for the application of multi-physics observers. Single metal foil and fiber-optic strain gauges were mounted at each of these locations to enable comparison of the performance of the two technologies. SNL has been performing metal-foil strain measurements of operational rotor blades for nearly four decades, but these sensors have never demonstrated the long-term reliability that would be needed for utility application. Fiber-optic strain measurements, on the other hand, are a fairly recent application for SNL, but they have been shown to continue to perform well at cycle counts well above those which are expected in the 20-year life of a turbine rotor blade. The fiber-optic temperature sensors will be used to study the correlation between rotor blade temperature and structural performance, hopefully yielding crucial insight into the role of temperature in the "noise" or randomness that is typically observed in the strain signals recorded during online structural health and condition monitoring.

The aerodynamic measurements were installed at approximately 7.9m (the center spanwise location of the aerodynamic modules) on each blade. These measurements include a traditional five-hole Pitot tube for determining angle of attack and velocity (presently on only one blade), as well as an array of pressure taps to measure the chord-wise distribution of surface pressure. Two modifications were made to minimize the difficulties that past users of similar aerodynamic measurements have experienced. First, the Pitot tube was built with an integrated bend to place it at the nominal angle of attack orientation to maximize the angular range and accuracy of the measurement. Second, a highly accurate absolute pressure sensor was located in each blade to measure the reference pressure, eliminating the complexity associated with the pneumatic slip-ring required for the usual hub-mounted absolute pressure reference.

Upon completing installation of the sensor arrays, TPI closed the blades and performed some final surface finish work. The blade set was then shipped to SNL in Albuquerque, NM.

B. Blade Modification

After receiving the blades from TPI Composites, SNL staff began modifying the blade structure so that the active control modules could be installed. The first step was to remove the portion of each blade corresponding to the intended location of the modules. A CAD software model of the geometry provided the surface measurements needed to accurately define the cutout. The most difficult challenge in drawing the layout lines was accommodating the variation exhibited among the three blades. Although the blade skins all came from the same mold, variations in material placement, assembly, and finishing operations resulted in noticeable differences in blade tip geometry and airfoil thickness. We adjusted the placement of the cutout to align with the Pitot tube port location and measurements made from the root and tip. Surface distance measurements were greatly simplified by using ruled adhesive tape having millimeter markings. A metal protractor with rotating

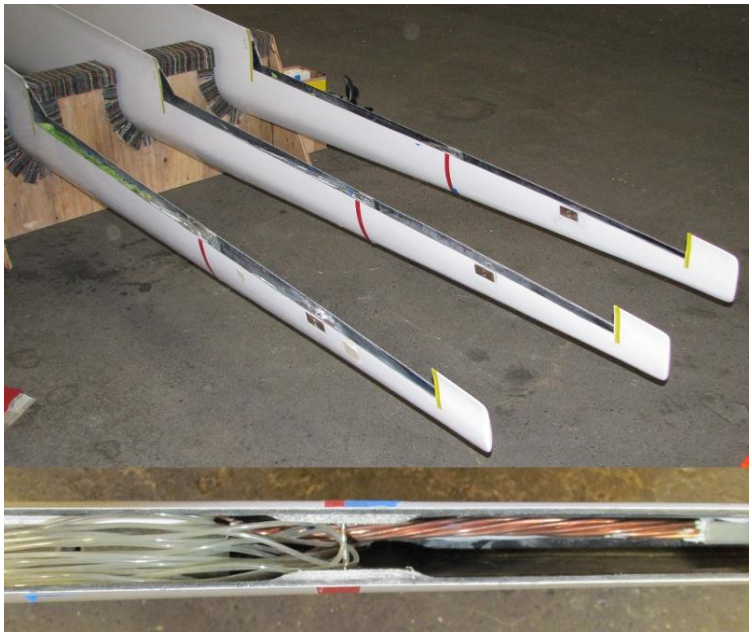

Figure 4. Top: blade set after removal of 6-foot section. Bottom: close-up of cavity showing surface pressure tap tubing and lightning cable.

straightedge was a useful aide in obtaining the appropriate angles in relation to the trailing edge of the blade. With the layout lines drawn, the blades were ready for removal of the trailing edge section.

We used a Rockwell Sonicrafter oscillating "multi-tool" with a semi-circular cutting attachment to cut through the skin material (approximately 3 mm thick) and remove the 6-foot long portion of the trailing edge. This tool was easy to control, accurate, and kicked up very little dust (although it was still necessary to have appropriate respiratory protection while cutting glass and carbon fiber). Figure 4 shows the modified blade set. After some finishing work on the rough edges, the blades were ready for the next step in the modification process.

The next step was to design and build a shear-web-like component to bridge between the upper and lower skins of the cavity and provide a flat surface for mounting the active control modules. In this paper, we refer to this component as the aft or secondary shear web. The CAD software model of the blade geometry allowed us to develop a rough initial design of the component which we then refined after the trailing edge cutout had been removed. The initial design was similar in concept to the main shear web of the blade: it had a C-channel shape with birch plywood core sandwiched between layers of biaxial carbon. However, upon removing the trailing edge cutout, we made two major changes to the initial design. First, we measured the cavity of each blade and modified the flanges of the secondary shear web to accommodate interior protrusions such as the lightning protection system and surface pressure taps. We also decided that the birch plywood core would complicate the fabrication and was actually unnecessary because the gap spanned by the web was small enough that carbon laminate alone would provide sufficient resistance against buckling of the web. We constructed a mold for the secondary shear web which established the tapering geometry of the C-channel. Features such as cable pass-thru holes and attachment point holes were also defined by the mold. This approach allowed these features to be located accurately relative to one another and relative to the overall shear web geometry. Attempting to add these features after the part was formed would have proved to be a difficult problem of accurately fixturing and locating the part for subsequent drilling and machining. We placed four layers of Vector Ply C-BX 1200 biaxial carbon cloth in the mold, orienting the biaxial fiber directions at +45 and -45 degrees relative to the centerline of the mold. To create the features previously discussed while also maximizing strength, as much as possible we avoided cutting the fibers but rather molded them around pegs which defined the hole features. In especially thin and weak areas, we added strands of uni-axial carbon fiber as reinforcement. The dry materials were then vacuum-infused with Hexion resin (system MGS RIMR 135 / RIMH 1366) to create the composite part. The final step in completing the shear webs was to add the attachment point hardware. We used #8-32 threaded nutplates from Click Bond (part numbers CN609CR08 and CN614CR08). The base of these nutplates bonds to the composite surface while the threaded portion is able to "float" a small amount within the base. This movement provides some leeway when attaching and aligning the modules.

We then bonded the secondary shear webs into place using Hexion structural adhesive (system BPR 135G / BPH 137G). Achieving proper alignment of the shear web was critical in this step so that the active modules would align with the surrounding blade surfaces. Because the shear webs themselves could twist and flex somewhat, we used a piece of aluminum bar stock to create a rigid jig which ran the full length of the shear web. At each end of the jig, we placed a cutout corresponding to the profile of the active module. For each blade we had to split the difference between these two reference points to achieve an overall average alignment of the geometry. During the installation process, we routed the motor control cables and the accelerometer cables through the shear web feed-thru holes and also routed the surface pressure tubing within the cavity. Immediately after applying the adhesive, we performed a pre-cure at 50 °C for 1 hour using a HEATCON power blanket while monitoring the temperature with a HEATCON 9200 Hot Bonder. Later, we post-cured the adhesive at 75 °C for 4 hours using the same equipment. Figure 5 shows the bonded secondary shear web with attachment points and cable feed-thru.

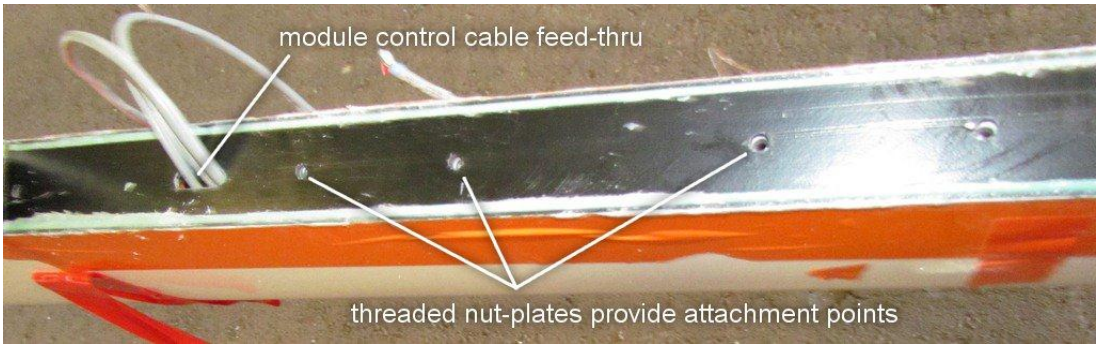

Figure 5. Secondary shear web bonded into place.

C. Flap Module Assembly

The flap modules' red flap pieces and the white base pieces were fabricated using a Fiber Deposition Modeling (FDM) rapid prototyping printer which produces complex geometry by building up layers of material. The material is P400 ABS plastic which has a density of 1.05 g/cm^3 and a tensile strength of 5000 psi (34.4 MPa). The surface quality of the parts is fairly smooth and depends somewhat upon the orientation of the surface with respect to the deposited layers, but we decided to sand the parts with fine-grit sand paper to produce a better finish with surface roughness closer to that of the blade skin. We also applied a coat of clear UV-resistant spray paint to the parts to slow down degradation of the plastic in sunlight.

We added some weather resistance to the motors by applying Plasti Dip® to the control wires where they protrude from the motor encoder and also encapsulated the entire encoder assembly. The connector which joins the motor to the blade control cables was also sealed to keep water away from the electrical contacts. At the root end of the blade control cables, mil-spec waterproof connecters join the cables to the control box.

After all nine modules were fully assembled, each set of three was installed on the blades. Each module was attached with six #8-32 cap head screws. Before tightening the screws, each module was positioned to align with the mating blade surface. Mismatch between the surfaces was smoothed out using a flexible filler compound. Figure 6 shows the completed blade set.

Figure 6. Fully assembled SMART blade set.

V. Control Loops and Hardware Implementation

There are three levels of control loops which govern operation of the active flap modules. The first and lowest level of control is the actuator control loop. This loop is responsible for driving each motor so that their shaft angles remain near the setpoints commanded by the other control loops. The actuator control operates at a high loop rate and must be able to respond to disturbance inputs acting on the motors. This means that the shaft angle must remain near the setpoint both when there is no torque load on the shaft and when there is a constant or variable torque input. The exact magnitude and characteristics of this torque input are unknown and therefore it is regarded as a disturbance entering the actuator control loop. Implementation of the actuator control loop depends upon the choice of actuator used in the modules. In the present implementation, the electric motors need motion control drives which provide both the control logic and the driving electronics that supply power to the motors. If the motors were replaced by servos, the control logic and electronics would be very similar but would be integrated with the motor package rather than existing in a separate drive package. For other types of active aerodynamic modules, the actuator may look very different, say pneumatic or hydraulic or piezoelectric, and the actuator control loop implementation would also be different.

In the present flap module implementation, the electric motor is a Faulhaber series 2642W024CR dc motor with a 26/1S series gearhead having a reduction ratio of 66:1. The actuator control loop requires a position feedback sensor, and we chose a Faulhaber series IE3-512L magnetic encoder to provide this feedback. It is an incremental encoder, meaning that the encoder signal does not indicate an absolute position but rather a change in position. There are three encoder output signals. One is an index pulse which occurs once every revolution of the motor shaft (and about 66 times every revolution of the gearhead output shaft). The other two outputs constitute a typical quadrature encoding scheme in which the two signals look like square waves which are 90 degrees out of phase. The square wave pulses are generated by the 512 encoder lines (pulses) per revolution. With this setup, the theoretical maximum positioning resolution of the gearhead output shaft is 0.003 degrees (but backlash in the gears will reduce the accuracy somewhat). This encoder has a "line driver" which produces differential rather than single-ended signal outputs. The differential signals tend to reject electromagnetic interference and this allows the encoder signal to be transmitted down the length of the blade to the motor position controller located at the hub.

We chose to use the Maxon EPOS2 24/5 positioning control unit to drive each motor. This motor driver can supply 5 amps continuously and 10 amps intermittently at 24 volts, while the motor should require less than 2 amps for most flap motions and loading conditions. In this motor driver, the actuator control loop has a switching frequency of 50 kHz (this is the rate at which the drive pulses power to the motor) and a positioning controller update rate of 1 kHz. The position controller is a PID regulator with velocity and acceleration feedforward factors. The Maxon EPOS Studio software provides a utility for automatic tuning of the PID gains. In addition to the position control function, each EPOS2 unit implements safeguards and limits to keep the motor within a specified operating range. The drive can also provide feedback on motor states such as position, velocity, and current.

The second of the three levels of control loops sits above the actuator control loop and is responsible for transitions between various system operating states. We will call this loop the state controller. It ensures that all of the motor drives are in the same operating mode and it responds to state transition commands from the top level master controller. When the system first powers up, the state controller polls the motor drives and causes them to lock the flaps in their current position. When signaled by the master controller, the state controller then tells the motor drives to perform a homing operation which zeros the flaps. It polls the drives to verify homing is complete and then the waits for the signal to begin accepting position commands. It is always running and handling drive faults that may occur, even when the master controller is idle or being reconfigured. We implemented the state controller in a set of three Freescale microcontrollers.

The third level control loop is the master controller. In addition to the signaling operations which have already been mentioned, the master controller is responsible for generating the position setpoint command for each flap module. For open-loop control this may be sinusoidal motions or step movements. For closed-loop control it will take information from the rotor sensor network and continually make flap control decisions according to the programmed control law. The master controller has been implemented with an Athena single-board computer from Diamond Systems. This embedded computer runs a real-time operating system which is programmed within the Matlab/Simulink xPC Target framework. The Athena provides analog-to-digital and digital-to-analog conversion as well as digital I/O interfaces. Position control commands are currently being given to the motor drives via analog signals because we found that the Athena could not send RS-232 messages fast enough to all nine motor drives. Switching to a faster communication protocol such as CAN bus may resolve this problem.

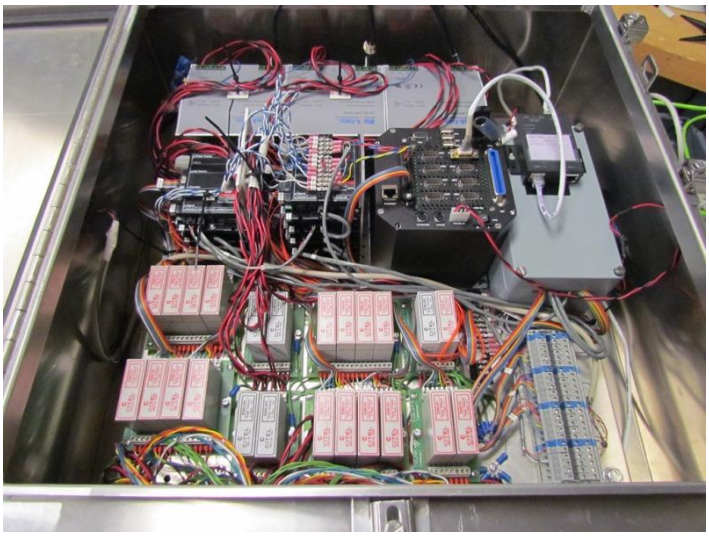

Figure 7. SMART rotor control box containing power supplies, lightning protection, motor drives, and controllers.

Figure 7 is a picture of the control box containing power supplies, lightning protection on all input lines, the Maxon motor drives, the Freescale microcontrollers, the Athena single-board computer.

VI. Testing

As of December 2011, we have performed ground calibration tests on all three blades and initial system checkouts with the rotor mounted on the turbine. The ground calibrations are a key part of the process in developing an accurate structural dynamics model of the operating rotor. First, the foil strain gauge bridges were zeroed to ensure an accurate strain reference. Next, static pull tests in the flap and edge directions characterize the strain and displacement distributions under specific proof loads. Finally, modal tests with two different support configurations (cantilevered and free-free) characterize the natural bending shapes, frequencies, and damping. Parameter extraction techniques allow us to estimate the blade stiffness distribution from the modal response data.

Table 1 gives preliminary results of the free-free modal test. Five flexible modes were calculated in addition to three rigid body modes.

Table 1. Natural frequency and damping values of the SMART blades with free-free supports.

Mode	Blade 1		Blade 2		Blade 3		Average		Mode Shape
Number	Freq (Hz)	Damp (% Cr)	Freq (Hz)	Damp (% Cr)	Freq (Hz)	Damp (% Cr)	Freq (Hz)	Damp (% Cr)	Description
RB1	0.25	6.0	0.26	5.8	0.26	5.9	0.26	5.93	Rigid Body Horizontal Twist (about Y-Axis)
RB2	0.31	3.9	0.29	4.8	0.33	3.5	0.31	4.07	Rigid Body Vertical Twist (about X-Axis)
RB3	2.69	1.0	2.62	1.4	2.61	0.6	2.64	1.02	Rigid Body Longitudinal Twist (about Z-Axis)
1	7.28	0.5	7.19	0.5	7.21	0.6	7.23	0.53	First Flap Bending
2	15.91	1.1	15.63	1.0	15.74	1.2	15.76	1.12	First Edge Bending
3	17.92	1.0	17.57	0.9	17.73	1.0	17.74	0.96	Second Flap Bending
4	29.27	1.5	29.21	1.1	29.52	0.9	29.33	1.15	Third Flap Bending
5	36.68	1.5	35.93	1.7	37.44	0.4	36.68	1.22	Second Edge Bending

While Blade 1 was cantilevered to the test fixture, the flaps were commanded with a sinusoidal waveform in which the frequency swept from 0.2 Hz to 10 Hz in a logarithmic fashion. Figure 8 shows the blade response at the mid-span location and the flap position response. The magnitude of the flap position response was constant until the position command input reached a frequency of about 6.4 Hz. At this point, a resonant mode of the actuation system was excited and the flap response magnitude increased above the input command magnitude. Above this frequency, the response magnitude quickly tapered off. During the test, it was obvious from blade tip motion that at least two blade modes were excited during the frequency sweep and the 4.5m span strain gauge clearly recorded what was observed visually. Figure 9 shows the same data channels in the frequency domain and reveals that cantilevered blade modes were excited by the command input at 3.3 Hz, 4.0 Hz, and 8.0 Hz.

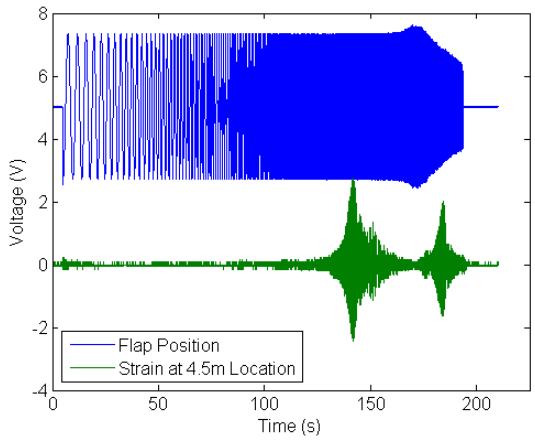

Figure 8. Blade response due to flap excitation.

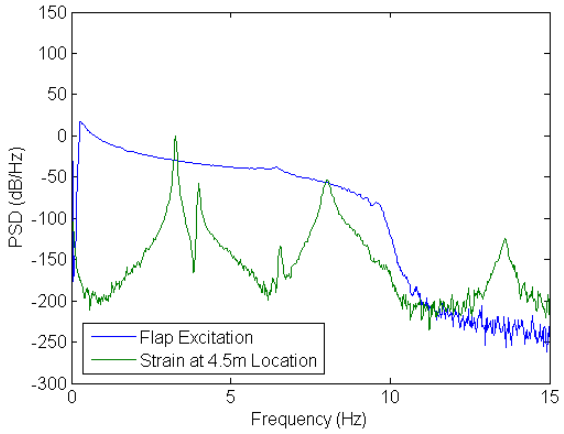

Figure 9. Power spectral density of motor excitation and blade response

Plans for future tests involve a number of phases. The first phase includes swept sine flap excitation on the parked rotor and slow rolls of the rotor to checkout the sensing systems. The second phase involves motored operation of the rotor at reduced speed (around 20 rpm) with both static and dynamic flap actuation. The final phase is power-generating operation at full speed, again with both static and dynamic flap actuation.

Acknowledgments

The authors gratefully acknowledge Brian Resor, Josh Paquette, David Wilson and Mark Rumsey of SNL for their contributions to the blade design, modifications, and controllers as well as Wesley Johnson and Bruce LeBlanc of SNL and Nathanael Yoder of ATA Engineering for their contributions during ground calibrations and data post processing.

References

[1]Barlas, T.K. and van Kuik, G.A.M., Review of state of the art in smart rotor control research for wind turbines, *Progress in Aerospace Science (2009)*, doi:10.1016/j.paerosci.2009.08.002

[2]van Wingerden, J-W., Hulskapp, A.W., Barlas, T., Marrant, B, van Kuik, G.A.M., Molenaar, D-P, and Verhaegen, M., On the Proof of Concept of a 'Smart' Wind Turbine Rotor Blade for Load Alleviation, Wind Energy, 2008; 11:265-80.

[3]Barlas, T., van Wingerden, J-W, Hulskamp, A, and van Kuik, G, "Closed-loop Control Wind Tunnel Tests on an Adaptive Wind Turbine Blade for Load Reduction," *Proceedings of the 46th AIAA/ASME*, Reno, NV, USA, 2008.

[4]Troldborg, N., Computational study of the Risø B1-18 airfoil with a hinged flap providing variable trailing edge geometry. *Wind Engineering* 2005, 29:89-113.

[5]Buhl, T., Gaunaa, M., and Bak, C., "Load reduction potential using airfoils with variable trailing edge geometry," *Proceedings of the 43th AIAA/ASME*, Reno, NV, USA, 2005.

[6]Buhl, T., Gaunaa, M., and Bak, C., Potential load reduction using airfoils with variable trailing edge geometry. *Solar Energy Engineering* 2005, 127:503-16.

[7]Andersen, P. B., Gaunaa, M., Bak, C., and Buhl, T., "Load alleviation on wind turbine blades using variable airfoil geometry," *Proceedings of the EWEC* 2006, Athens, Greece.

[8]Andersen, P. B., Gaunaa, M., Bak, C., and Buhl, T., "Wind tunnel test on wind turbine airfoil with adaptive trailing edge geometry," *Proceedings of the 45th AIAA/ASME*, Reno, NV, USA, 2007.

[9]Buhl, T., "Stability Limits for a Full Wind Turbine Equipped with Trailing Edge Systems," European Wind Energy Conference, Marseille, France, 16-19 March, 2009.

[10]Anderson, P.B., "Load Reduction Using Pressure Difference on Airfoil for Control of Trailing Edge Flaps," European Wind Energy Conference, Marseille, France, 16-19 March, 2009.

[11]Wilson, D.G., Berg, D.E., Barone, M.F., Berg, J.C., Resor, B.R., and Lobitz, D.W., "Active Aerodynamic Blade Control Design for Load Reduction on Large Wind Turbines" European Wind Energy Conference, Marseille, France, 26-19 March, 2009.

[12]Berg, D.E., Wilson, D.G., Barone, M.F., Berg, J.C., Resor, B.R., Paquette, J.A., and Zayas, J.R., "The Impact of Active Aerodynamic Load Control on Fatigue and Energy Capture at Low Wind Speed Sites," European Wind Energy Conference, Marseille, France, 16-19 March, 2009.

[13]Berg, D.E., Wilson, D.G., Resor, B.R., Barone, M.F., Berg, J.C., Kota, S. and Ervin, G., "Active Aerodynamic Blade Load Control Impacts on Utility-Scale Wind Turbines," WINDPOWER 2009, Chicago, Illinois, 5-7 May, 2009.

[14]Wilson, Berg, D.E., D.G., Resor, B.R., Barone, M.F., and Berg, J.C., "Combined Individual Pitch Control and Active Aerodynamic Load Controller Investigation for the 5MW UpWind Turbine, WINDPOWER 2009, Chicago, Illinois, 5-7 May, 2009.

[15]Resor, B., Wilson, D., Berg, D., Berg, J. , Barlas, T., and van Kuik, G., "The Impact of Higher Fidelity Models on Active Aerodynamic Load Control Fatigue Damage Reduction," *Proceedings of the 48th AIAA Aerospace Sciences Meeting*, Orlando, FL, January 4-7, 2010.

[16]Wilson, D.G., Resor, B.R, Berg, D.E., Barlas, T.K., and van Kuik, G.A.M., "Active Aerodynamic Blade Distributed Flap Control Design Procedure for Load Reduction on the UpWind 5MW Wind Turbine," *Proceedings of the 48th AIAA Aerospace Sciences Meeting*, Orlando, FL, January 4-7, 2010.

[17]Berg, D. E., Wilson, D., Resor, B., Berg, J., Barlas, T., Crowther, A. and Halse, C., "System ID Modern Control Algorithms for Active Aerodynamic Load Control and Impact on Gearbox Loading," The Science of Making Torque from Wind, 2010.

[18]Berg, D., Berg, J., Wilson, D., White, J., Resor, B., and Rumsey, M., "Design, Fabrication, Assembly and Initial Testing of a SMART Rotor," *Proceedings of the 49th AIAA Aerospace Sciences Meeting*, Orlando, FL, January 4-7, 2011.

[19]Berry, D. and Ashwill, T., "Design of 9-Meter Carbon-Fiberglass Prototype Blades: CX-100 and TX-100," SAND2007-0201, September 2007, Sandia National Laboratories, Albuquerque, NM

[20]Zayas, J.R., Jones, P.L., and Holman, A., "CX-100 and TX-100 Blade Field Tests," SAND05-7454, December 2005, Sandia National Laboratories, Albuquerque, NM

[21]Paquette, J., Laird, D.L., Griffith, D.T., and Rip, L., "Modeling and Testing of 9m Research Blades," *Proceedings of the 44th AIAA Aerospace Sciences Meeting*, Reno, NV, January 2006

[22]Paquette, J., van Dam, J., Hughes, S., "Structural Testing of 9m Carbon Fiber Wind Turbine Research Blades," *Proceedings of the 45th AIAA Aerospace Sciences Meeting, Reno*, NV, January 2007

[23]White, J., Adams, D., Rumsey, M., "Measurement of Operational Loading and Deflection with a Smart Turbine Rotor Blade," WINDPOWER 2009, Chicago, IL, May 4-7, 2009.